Laser-assisted Simulation of Dose Rate Effects of Wide Band Gap Semiconductor Devices

TANG Ge[1,2], XIAO Yao[1], SUN Peng[3], LIU Jingrui[1], ZHANG Fuwang[1], LI Mo[2,*]
(1. *Chengdu University of Technology*, *Chengdu* 610059, *China*;
2. *University of Electronic Science and Technology of China*, *Chengdu* 610054, *China*;
3. *Microsystem & Terahertz Research Center of CAEP*, *Chengdu* 621000, *China*)

Abstract: Laser-assisted simulation technique has played a crucial role in the investigation of dose rate effects of silicon-based devices and integrated circuits, due to its exceptional advantages in terms of flexibility, safety, convenience, and precision. In recent years, wide band gap materials, known for their strong bonding and high ionization energy, have gained increasing attention from researchers and hold significant promise for extensive applications in specialized environments. Consequently, there is a growing need for comprehensive research on the dose rate effects of wide band gap materials. In response to this need, the use of laser-assisted simulation technology has emerged as a promising approach, offering an effective means to assess the efficacy of investigating these materials and devices. This paper focused on investigating the feasibility of laser-assisted simulation to study the dose rate effects of wide band gap semiconductor devices. Theoretical conversion factors for laser-assisted simulation of dose rate effects of GaN-based and SiC-based devices were been provided. Moreover, to validate the accuracy of the conversion factors, pulsed laser and dose rate experiments were conducted on GaN-based and SiC-based PIN diodes. The results demonstrate that pulsed laser radiation and γ-ray radiation can produce highly similar photocurrent responses in GaN-based and SiC-based PIN diodes, with correlation coefficients of 0.98 and 0.974, respectively. This finding reaffirms the effectiveness of laser-assisted simulation technology, making it a valuable complement in studying the dose rate effects of wide band gap semiconductor devices.

Key words: laser-assisted simulation; dose rate effect; wide band gap semiconductor; conversion factor

CLC number: TL81 **Document code**: A **Article ID**: 1000-6931(2023)12-2314-12

doi: 10.7538/yzk.2023.youxian.0558

Received Date: 6 August 2023; **Revised Date**: 6 September 2023

Funding: National Natural Science Foundation of China (12205028); Natural Science Foundation of Sichuan Province (2022NSFSC1235); Young and Middle-aged Backbone Teacher Foundation of Chengdu University of Technology (10912-JXGG2022-08363)

* **Corresponding Author**: LI Mo

Wide band gap semiconductor (WBGS) materials exhibit excellent ionization radiation resistance due to their strong bonding and high ionization energy[1-2]. As a result, devices based on WBGS have been widely used in various application scenarios, particularly in nuclear industry, aerospace, and high-energy physics. Investigating the radiation resistance in WBGS devices, specifically their transient electrical performance under γ-ray radiation, often relies on ground-based facilities such as flash X-ray machines and linear accelerators to ensure the requisite radiation resistance characteristics. However, the limited availability, high cost, long testing cycle, and scarcity of data severely hinder the utilization of the above facilities. Fortunately, the devices exhibit similar photocurrent response under laser irradiation and dose rate irradiation[3-5]. This makes the laser-assisted simulation technology plays a significant role in the hardness assurance of devices.

A pulsed laser has been effectively used to simulate dose rate effects on silicon-based devices due to its stable pulse output, low cost, simple operation, and ionizing radiation safety for users. Combining the advantages of tunable laser parameters, such as wavelength, repetitive frequency, and laser spot size, the laser-assisted simulation system enables a more accurate study of the carrier transportation process in semiconductor devices. Additionally, the laser can be focused onto specific sensitive units of the device or circuit, making it well-suited for identifying areas of weakness. Thanks to these unique advantages, the laser-assisted simulation technique provides essential laboratory test methods for the radiation resistance design, diagnosis, and failure mechanism research of semiconductor devices and integrated circuits.

Currently, the feasibility of using pulsed laser to simulate dose rate effects of silicon-based PN junction, bipolar junction transistor (BJT), metal oxide semiconductor (MOS) and other devices has been verified[6-8]. With the expeditious development of semiconductor material systems, there is a pressing need to study the laser-assisted simulation technique for WBGS materials and devices. However, WBGS materials possess larger band gap, requiring higher ionization energies to generate excess electron-hole pairs. Compared to narrow band gap materials, WBGS materials generate fewer excess carriers at the same dose rate. Consequently, the photocurrent signal is easily to be overwhelmed by noise signal, resulting in a lower signal-to-noise ratio, which is unfavorable for laser-assisted simulation. Moreover, for WBGS materials, a shorter laser wavelength is necessary to generate excess electron-hole pairs. However, this leads to a shallower effective penetration depth for laser, which may cause significant differences in the distributions of carriers when the WBGS devices are irradiated by pulsed γ-ray and pulsed laser. Furthermore, dramatic differences in refractive index or absorption coefficient between WBGS materials and silicon-based materials can prevent the laser from reaching the active region of devices, thereby reducing the accuracy of laser-assisted simulation and potentially rendering it ineffective.

Besides, the variation in band gap type may also become a factor affecting laser-assisted simulation. In direct band gap materials, the conduction band minimum (CBM) and the valence band maximum (VBM) are located at the same k-space point, resulting in zero net momentum during electron transitions. On the other hand, for indirect band gap materials, the CBM and VBM are not at the same k-space point[9]. In general, transitions are more likely to occur in direct band gap materials during energy absorption. It is important

to note that both GaN and SiC are typical WBGS materials, which are different from silicon as an indirect band gap material. Additionally, the recombination mechanisms differ between direct and indirect band gap materials. For example, radiative recombination probability is significantly higher in direct band gap materials than in indirect band gap materials. These variations make it challenging to precisely determine the extent to which specific factors affect laser-assisted simulation.

To investigate the impact of these variations and assess the feasibility of laser-assisted simulation of dose rate effects of WBGS devices, this paper describes a carrier generation model in WBGS materials. It analyzes the proportion of linear and nonlinear absorption, and provides a calculation method of the conversion factor. Furthermore, to ensure the validity of the laser-assisted simulation, GaN-based and SiC-based PIN diodes are tested using both a pulsed γ-ray source and a pulsed laser source, respectively.

1 Theory

1.1 Photocurrent generation of WBGS under pulsed γ-ray

When WBGS materials are exposed to γ-ray ionizing radiation, a phenomenon known as the Compton effect takes place. During this process, the materials absorb a portion of photon energy leading to the generation of electron-hole pairs. These excess charge carriers then contribute to the generation of photocurrent under the influence of electric field forces. The photocurrent generated by the excess charge carriers can have an impact on the normal operation of devices. In certain circuit structure, this photocurrent may be amplified, further exacerbating its effects. When the radiation source is removed, the excess charge carriers exhibit higher mobility and recombination rates[10]. Over time, these excess charge carriers gradually return to equilibrium, and restoring the material to its original state.

The absorption of γ-ray radiation by WBGS materials can be generally divided into two parts. One portion of the energy is converted into lattice vibration, or phonons, resulting in an increase in material's temperature. The remaining energy is utilized to generate electron-hole pairs through the photoelectric effect. The above energy that is of our concern, which gives rise to electron-hole pairs, is commonly referred to as the average ionization energy (E_i). Relevant reference has shown a strong correlation between the E_i and the band gap width (E_g) of the material[11]. This correlation can be utilized to estimate the E_i of semiconductor materials. For instance, the E_g of Si, 3C-SiC, and GaN are 1.12, 2.3, and 3.4 eV, respectively. Accordingly, the corresponding E_i are approximately 3.6, 6.9, and 8.9 eV, as listed in Table 1. The relationship between the E_i and the E_g of WBGS materials can be expressed as follows:

$$E_i = 2.8E_g + 0.6\ \text{eV} \tag{1}$$

The generation rate (G_γ) of excess charge carriers can be expressed as follows[12]:

$$G_\gamma = g_0 P_\gamma \tag{2}$$

where P_γ is the γ-ray dose rate and g_0 is the generation constant. For g_0, it is related to E_i and the density (ρ) of the WBGS material. It can be approximately calculated using the following formula[13]:

$$g_0 = \frac{10^{14}\rho}{1.6E_i} \tag{3}$$

By combining Eq. (1) and Eq. (3), the relationship between ρ, E_g, and the g_0 can be obtained as shown in Eq. (4).

$$g_0 = \frac{10^{14}\rho}{4.48E_g + 0.96} \tag{4}$$

Using the Eq. (4), the calculated values of the g_0 are listed in Table 1 alongside the corresponding parameters of several typical

Table 1 Several typical physical characteristic of semiconductor material

Physical parameter	Parameter value of semiconductor material					Reference
	Si	SiC	GaN	Al_2O_3	Ga_2O_3	
E_g, eV	1.12	2.3(3C-SiC)	3.4	8.8(α-Al_2O_3)	5.2(α-Ga_2O_3)	[10,14-16]
		2.9(4H-SiC)		5.1-7.1(am-Al_2O_3)	4.9(β-Ga_2O_3)	
		3.2(6H-SiC)		7.0-8.7(γ-Al_2O_3)		
E_i, eV	3.6	6.9	8.9	8.9	13	[11,17-19]
ρ, g·cm^{-3}	2.3	3.21	6.15	3.9	5.9	[19-23]
g_0, 10^{13} pairs·rad^{-1}·cm^{-3}	4.3	2.85	3.8	0.97	2.4	[12]

Note: In the rows labeled "E_g", the characters in parentheses denote the crystal structure type of the materials

WBGS materials for comparison with Si as a reference material.

1.2 Photocurrent generation of WBGS under pulsed laser

Laser radiation and γ-ray radiation differ significantly in terms of their photon energy. However, in scenarios involving laser radiation, the photoelectric effect becomes the primary mechanism for generating electron-hole pairs, leading to the production of photocurrent. Despite the distinct mechanisms involved, lasers can effectively simulate the dose rate effects observed in WBGS devices. This is attributed to their comparable electrical response and strong correlation with the effects induced by γ-ray irradiation.

The generation of photocurrent in semiconductor materials by laser irradiation involves complex energy transfer mechanisms. When the photon energy of laser exceeds the band gap of the material, there are primarily two absorption mechanisms depending on the number of photons absorbed per electron-hole pair generated: linear absorption and nonlinear absorption. The intensity of the laser at a penetration depth z(cm) within the material, denoted as I(W·cm^{-2}), can be expressed as follows:

$$I(z)=\frac{I_0 e^{-\alpha z}}{1+\frac{\beta I_0}{\alpha}(1-e^{-\alpha z})} \tag{5}$$

where I_0 is the incident light intensity at the surface of the material ($z=0$); α is the linear absorption coefficient, cm^{-1}, primarily influenced by intrinsic absorption; β represents the nonlinear absorption coefficient, cm·W^{-1}, predominantly affected by two photon absorption (TPA).

Then the carrier generation rate G_L within the material can be expressed by the following equation:

$$G_L=\alpha_i\frac{I(z)}{h\nu}+\beta\frac{I^2(z)}{2h\nu} \tag{6}$$

where $h\nu$ is the photon energy and α_i is the intrinsic absorption coefficient ($\alpha_i\approx\alpha$).

In practical experiments, it is possible to estimate the contribution of TPA by calculating the $\beta I_0/\alpha_i$ as indicated in Eq. (5)[24]. Taking GaN as an example, under the irradiation conditions of a laser wavelength of 355 nm, α_i is approximately 10^4 cm^{-1}, and β is approximately 10^{-8} cm·W^{-1}. When the I_0 is 10^7 W·cm^{-2}, the excess carrier generation due to TPA accounts for approximately 0.001% of the carrier generation from one-photon absorption. Therefore, the second term in Eq. (6) can be neglected. The relevant properties of other materials can be found in Table 2, and the G_L of GaN can be simplified as:

$$G_L\approx\frac{I_0\alpha_i e^{-\alpha_i z}}{\left[1+\frac{\beta I_0}{\alpha_i}(1-e^{-\alpha_i z})\right]h\nu} \tag{7}$$

For SiC devices, since the $\beta I_0/\alpha_i$ of SiC is

Table 2 Linear and nonlinear absorption coefficient of several semiconductor materials

Physical parameter	Parameter value of semiconductor material				Reference
	Si	SiC	GaN	Al_2O_3	
laser wavelength, nm	1 064	532	355	192	[25-29]
α_i, cm^{-1}	14	$\sim 10^4$	$\sim 10^4$	$\sim 10^4$	
β, $cm \cdot W^{-1}$	3×10^{-8}	$\sim 10^{-4}$	$\sim 10^{-8}$	$\sim 10^{-4}$	
$\beta I_0/\alpha_i$ ($I_0=10^7\ W\cdot cm^{-2}$)	2.1×10^{-2}	10^{-1}	10^{-5}	10^{-1}	[24]

Note: Due to the variation in doping levels in SiC, GaN, and Al_2O_3, the values of α_i and β are not exact, therefore the symbol "～" is used to indicate that α_i and β are in a certain order of magnitude

0.1, TPA needs to be considered.

1.3 Calculation of conversion factor for WBGS

The conversion factor (CF), which is an essential parameter for evaluating the equivalence between laser radiation and γ-ray radiation, plays a significant role in laser-assisted simulation experiments of WBGS devices. Currently, there are three methods available for determining the CF, each based on different reference standards. These methods include the calculation using the carrier generation rate (CGR)[12], peak photocurrent equivalent (PPE)[3], and charge collection equivalent (CCE)[4]. Each of these methods offers a distinct equivalent basis for assessing the similarity between laser radiation and γ-ray radiation.

Take the method of CGR as an example, the calculation method of the CF based on CGR was proposed by Nikiforov et al[12]. According to the mechanisms described in sections 1.1 and 1.2 regarding the effects of γ-ray radiation and laser radiation on WBGS materials, when considering the excess carriers as the equivalent basis, if,

$$G_L = G_\gamma \tag{8}$$

It can be considered that the laser radiation and γ-ray radiation are equivalent in terms of their parameters, and the dose rate corresponding to the laser power density (P_L), is referred to as the equivalent dose rate (P_{eq}). And its relation expression is:

$$P_{eq} = CF \cdot P_L \tag{9}$$

By combining Eq. (2) and Eq. (7), the average value of CF is given by:

$$CF = \int_0^w \frac{\alpha_i e^{-\alpha_i z}}{\left[1+\frac{\beta I_0}{\alpha_i}(1-e^{-\alpha_i z})\right] h\nu g_0 w} dz \tag{10}$$

where w is the sensitive region thickness, the w value of 100 nm, the α_i value of 80 000 cm^{-1}, the β value of 7×10^{-9} $cm\cdot W^{-1}$, and the $h\nu$ value of 5.6×10^{-19} J, the calculated CF for GaN is approximately 2.59×10^9 rad(Si)·s^{-1}/(W·cm^{-2}) according to the above equation.

The methods of PPE and CCE are different from the theoretical methods of CGR, they all rely on actual γ-ray experimental data. The PPE method will be detailed introduction in the results and analysis section.

2 Device description and experimental setup

2.1 Device description

The GaN-based and SiC-based PIN diodes are both encased in metal packaging with three pins representing the cathode, anode, and grounding (connected to the shell). In order to assess their performance under transient γ-ray radiation and pulsed laser radiation, it is necessary to remove the packaging and expose the internal components of the devices. The unpacked device layouts, which are observed under a microscope, are shown in Fig. 1.

The active area of the GaN-based device

(W1) is a square with a side length of 1 150 μm, whereas the active area of the SiC-based device (W2) is circular with a diameter of 135 μm. Both W1 and W2 have an active region depth of at least 100 nm. The specific device structure parameters are illustrated in Fig. 2. Taking W1 as an example, the heavily doped top layer combines with a metal electrode to form a P-type ohmic contact. The P-GaN region is combined with N-GaN to create a PN junction. Additionally, the I-GaN layer serves as a transition region, facilitating charge balance and current flow limitation. For W2, the stepped P-region with doping concentration of 2×10^{17} cm^{-3} is mainly designed for high voltage resistance and breakdown resistance.

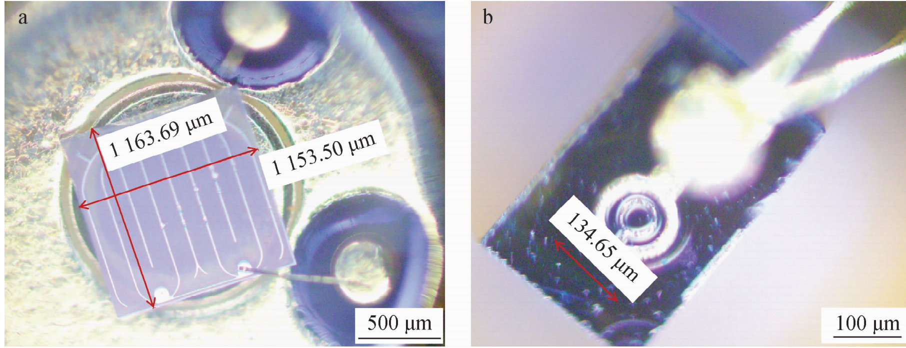

a—GaN-based PIN; b—SiC-based PIN

Fig. 1 Layout image of WBGS device

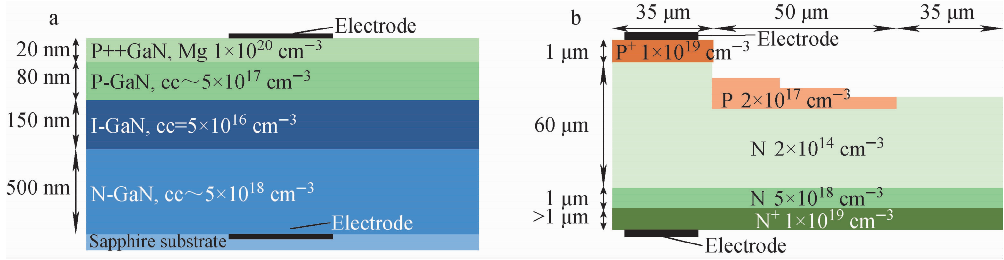

a—GaN-based PIN; b—SiC-based PIN

Fig. 2 Structure diagram of GaN-based and SiC-based PIN diodes

For a laser with a wavelength of 355 nm, the α of GaN and SiC are 80 000 cm^{-1} [30] and 225 cm^{-1} [31], respectively. Fig. 3 illustrates the relationship between the z of GaN and SiC materials and the normalized optical power density. As the z increases, the normalized optical power density decreases to 1/e (approximately 0.37). In the case of GaN, the z is approximately 100 nm, while for SiC, it is around 50 μm. Consequently, the laser with a wavelength of 355 nm can effectively meet the requirements for W1 and W2.

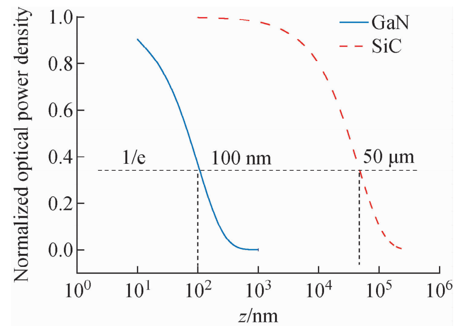

Fig. 3 Relationship between penetration depth and normalized optical power density for GaN and SiC

2.2 Experimental setup

The introduction describes the limitations

of traditional 532 or 1 064 nm lasers for WBGS materials. These materials, such as GaN, require lasers with shorter wavelengths, specifically around 355 nm, for single-photon ionization absorption. However, this ultraviolet wavelength range is incompatible with the optical lenses, detection, and imaging systems in the original ionizing effect laser-assisted simulation (IELS) system, which operates at 532 or 1 064 nm wavelengths[5]. To address these limitations, the wide band gap ionizing effect laser-assisted simulation (w-IELS) system was designed based on the IELS system[6], as depicted in Fig. 4. The w-IELS system operates at a conventional wavelength of 355 nm, with an adjustable wavelength range of 210-2 400 nm. The laser spot can be adjusted using focusing lense or a beam expander, and the laser spot diameter is 3-4 mm to ensure completely and uniformly coverage of the surface of the tested device. The maximum output laser energy of the system is 5.1 mJ with a repetition rate of 1-20 Hz, and a pulse width of 4-7 ns. Furthermore, the stability of the pulse can be controlled within a 5% root mean square (RMS) variation. The system's optical path includes a short-wavelength pulsed laser passing through an attenuating optical path and being reflected towards a beam-splitter for splitting. A portion of the laser enters a power meter probe to calculate the device's energy, while the rest, combined with guiding light source, reaches the surface of the semiconductor device under tested. The guiding light source is aligned with the center of the laser spot, facilitating the imaging of the WBGS device test sample using a CCD camera.

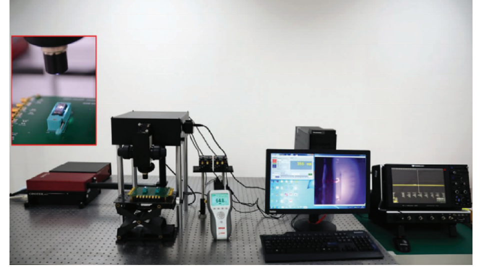

Fig. 4 Physical picture of w-IELS system

The dose rate experiments are conducted using the Qiangguang γ-ray generator from the State Key Laboratory of Intense Pulsed Radiation Simulation and Effect of China. The experimental setup is capable of generating γ-ray with a photon energy of 0.9 MeV. The pulse width can be varied within the range of 15-35 ns, and the spot size covers an area of 100 cm^2. The dose rate range is from 10^9 to 10^{11} rad(Si)/s. The basic experimental device layout is presented in Fig. 5[4].

In the test circuit, a reverse bias voltage of 5 V and a series resistance of 1 MΩ are chosen. The selection of this resistance is

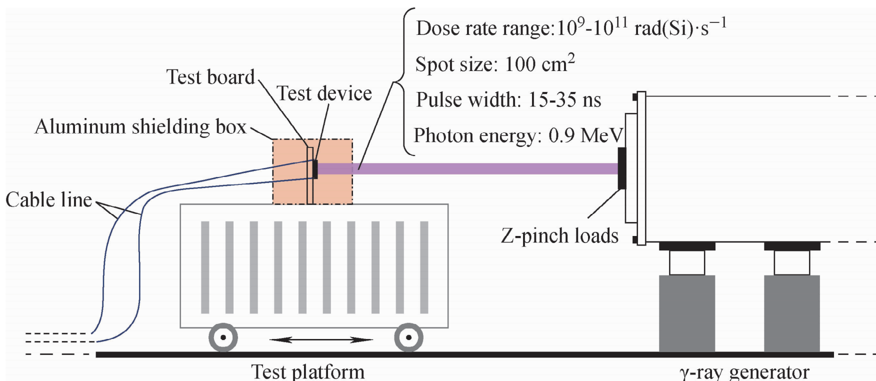

Fig. 5 Basic performance parameter of Qiangguang γ-ray generator

primarily based on the characteristics that WBGS materials require a higher mean ionization energy compared to silicon-based materials, resulting in a lower quantity of excess carriers being generated compared to silicon-based materials at the same dose rate. Consequently, a higher resistance is required to observe an obvious current response in WBGS materials. The GaN-based and SiC-based PIN diodes used in the experiment are small in size and have thin thicknesses. This leads to a weak electrical response generated at the dose rate, which can be easily overshadowed by noise. Taking these factors into consideration, a series resistance of 1 MΩ is determined to ensure an adequate current response. Before conducting the irradiation experiment, the *I-V* curves of the devices are tested, as shown in Fig. 6. The leakage currents of GaN-based and SiC-based PIN diodes are below the nA level, which made it convenient to measure the instantaneous current during the device irradiation under the reverse bias voltage of 5 V.

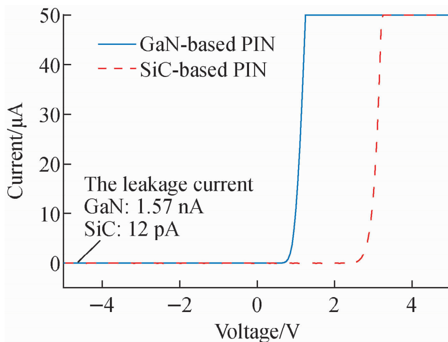

Fig. 6　*I-V* curve of GaN-based and SiC-based PIN diodes

3　Results and analysis

To establish the relationship between the photocurrent and two types of radiation (laser and γ-ray), a series of experiments are conducted. These tests involved measuring the peaks of response (I_{pp}) under varying laser intensities using the w-IELS system, as well as diverse γ-ray dose rates using the Qiangguang γ-ray generator. The photocurrent response curves of the GaN-based PIN under laser irradiation and γ-ray irradiation are depicted in Fig. 7 and Fig. 8.

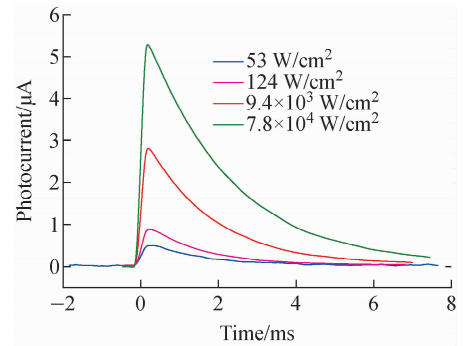

Fig. 7　Photocurrent response curve of GaN-based PIN under laser irradiation

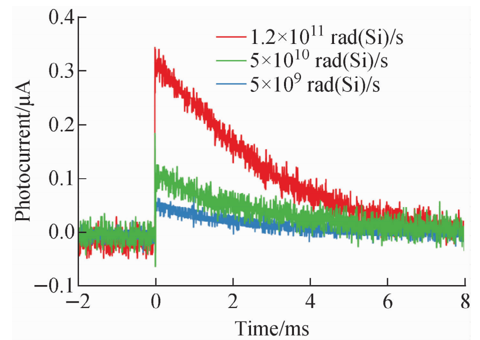

Fig. 8　Photocurrent response curve of GaN-based PIN under γ-ray irradiation

Given the maximum dose rate of Qiangguang γ-ray generator is approximately 1×10^{11} rad(Si)/s, the photocurrent peak remains below the μA level. Especially for GaN-based PIN, the photocurrents are even lower than 0.5 μA as shown in Fig. 8. In contrast, laser irradiation has the capability to simulate a much wider range of photocurrent response. Due to the need for matching of photocurrent peaks, the irradiation intensity range of both laser radiation and γ-ray radiation is selected based on the range of photocurrent generated by γ-ray radiation.

The calculation method of the CF based on the PPE method establishes a direct relationship between experimental and theoretical aspects. This method utilizes the peak photocurrent generated by both laser radiation and γ-ray radiation devices as the equivalence criterion. To determine the CF, it is essential to extract the I_{pp} value from the current curves obtained for each intensity level of the laser and γ-ray irradiated devices. The optimization technique is employed to solve for the CF, utilizing log-linear fitting and incorporating the specific relation of I_{pp} versus laser intensity and I_{pp} versus dose rate[6]. The expression for the optimized CF is as follows:

$$\mathrm{CF} = \underset{\mathrm{CF}_i}{\operatorname{argmin}} \| G(I_{pp}) - \mathrm{CF}_i \cdot F(I_{pp}) \|_2 \tag{11}$$

where $F(I_{pp})$ is the fitting function relating the laser power density to the peak photocurrent, and $G(I_{pp})$ is the fitting function relating the γ-ray radiation dose rate to the peak photocurrent. CF_i is a series of values within a predetermined range, and the optimal CF can be determined through calculation by Eq. (11). As shown in Fig. 9, CF_1, CF_2 and CF_3 are three suitable CFs, and CF_2 has the best fitting effect. So the CF for W1 is 4.5×10^8 rad(Si)·s^{-1}/(W·cm^{-2}). In comparison to the computed value using the CGR method, which is 2.59×10^9 rad(Si)·s^{-1}/(W·cm^{-2}), the value obtained by PPE is smaller. This is

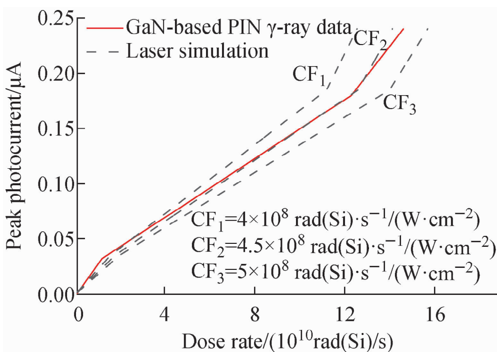

Fig. 9 Calculation process of GaN-based PIN equivalent coefficient

because, in practical experiments, most devices incorporate metal layers (electrodes) that obstruct a portion of incident light from entering the device and generating excess carriers. Additionally, as the laser wavelength increases, the z decreases, leading to energy dissipation before reaching the active region. The CGR method is difficult to account for these factors, so the CF is mainly calculated through PPE method in this study. Similarly, applying the Eq. (11) to W2 yields a CF of 9×10^7 rad(Si)·s^{-1}/(W·cm^{-2}).

Once the CF is obtained, it enables the simulation of a larger range of dose rates based on the results of laser irradiation and the CF. The specific laser-assisted simulation process involves testing the relationship between I_{pp} versus laser intensity using the w-IELS system, and then obtaining the equivalent dose rate from the product of laser intensity and CF, as described in Eq. (9). Fig. 10 presents the results of laser-assisted simulation for GaN-based and SiC-based PIN devices. The data points with error bars represent the experimental values of GaN-based and SiC-based PIN dose rates, while the points without error bars represent the calculated values. The highest dose rate achievable by the Qiangguang γ-ray generator limits the extent of the simulation. To address the problem, a finite-element method (FEM) is adopted in the numerical calculation to supplement high dose rate data, and the software platform is COMSOL Multiphysics 5.5. Additionally, the lines in Fig. 10 represent the simulation results obtained from laser radiation on GaN-based and SiC-based PIN devices. It is evident that the relationship between the peak photocurrent and the dose rate is consistent with the relationship between the peak photocurrent and the equivalent dose rate. At dose rates exceeding 10^{11} rad(Si)/s, the laser-assisted simulation technique continues to demonstrate

favorable performance. This shows that laser-assisted simulation can better simulate the peak photocurrent characteristic of WBGS devices. At the same time, due to the large adjustment range of laser intensity, the peak photocurrents of WBGS devices at high dose rates could be obtained without the help of FEM numerical simulation.

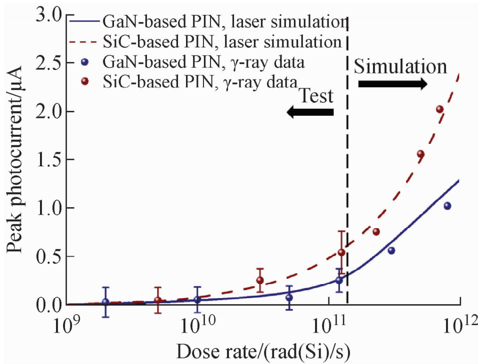

Fig. 10 Laser-assisted simulation result of GaN-based and SiC-based PIN devices

To further validate the accuracy of laser-assisted simulation, a dose rate of 1.2×10^{11} rad(Si)/s is selected to compare the actual photocurrent curves of WBGS PIN devices under laser radiation and γ-ray radiation, as shown in Fig. 11. The photocurrent responses generated by the laser and γ-ray in GaN-based and SiC-based PIN devices are very similar, and the correlation coefficients are 0.98 and 0.974, respectively. This further confirms that laser-assisted simulation technology is applicable to WBGS devices. As mentioned earlier, due to the influence of the absorption coefficient, short-wavelength lasers in GaN-based devices can only penetrate about 100 nm below the surface. Therefore, for GaN-based light-emitting diodes, laser diodes, and other multilayer devices with thick P-type layers and barrier layers, effectively applying laser-assisted simulation technology remains an urgent problem to be solved.

4 Conclusion

In this paper, the feasibility of laser-assisted simulation of the dose rate effects of WBGS devices is investigated. We have examined the peak photocurrent of WBGS devices under various laser intensities and γ-ray dose rates. By calculating the CF based on the relationship between the photocurrents induced by these two types of radiation, it becomes possible to use laser-assisted simulation to model the dose rate effects of WBGS devices. The results show that laser-assisted simulation is capable of more accurately simulating the peak photocurrent characteristic of WBGS devices, particularly at high dose rate. Moreover, the photocurrent responses of GaN-based and SiC-based PIN diodes under dose rate radiation can be simulated accurately by laser-assisted simulation, and the experimental results of the two

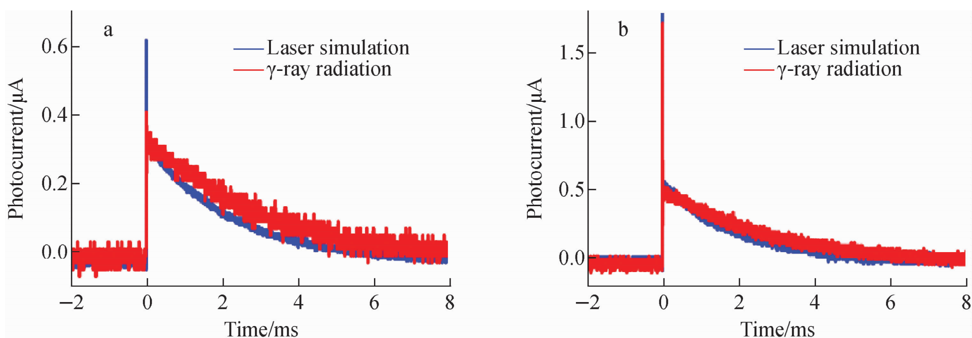

a—GaN-based PIN; b—SiC-based PIN

Fig. 11 Response curve of WBGS PIN devices under laser radiation and γ-ray radiation

are in good agreement.

Acknowledgements: The authors would like to thank Li Qian and Kang Jianbin from the Microsystem & Terahertz Research Center of CAEP, Chengdu, China, for their technical support; Wang Chenhui and Li Ruibin from the State Key Laboratory of Intense Pulsed Radiation Simulation and Effect, Xi'an, China, for their help during the γ-ray radiation experiments.

References:

[1] KIM J, PEARTON S J, FARES C, et al. Radiation damage effects in Ga_2O_3 materials and devices[J]. Journal of Materials Chemistry C, 2019, 7(1): 10-24.

[2] TSAO J Y, CHOWDHURY S, HOLLIS M A, et al. Ultrawide-bandgap semiconductors: Research opportunities and challenges[J]. Advanced Electronic Materials, 2018, 4(1): 1600501.

[3] NATION S A, MASSENGILL L W, MCMORROW D, et al. Laser dose-rate simulation to complement LINAC discrete device data[J]. IEEE Transactions on Nuclear Science, 2008, 55(6): 3 114-3 121.

[4] TANG G, LI M, SUN P, et al. A charge collection equivalent method for laser simulation of dose rate effects with improved performance[J]. IEEE Transactions on Nuclear Science, 2021, 68(6): 1 235-1 243.

[5] TANG G, SUN P, KANG J, et al. Laser-assisted simulation of dose-rate effects of neutron-irradiated NPN transistors[J]. IEEE Transactions on Nuclear Science, 2022, 69(5): 1 167-1 175.

[6] TANG G, LI M, SUN P, et al. Surface metallization influence on equivalence of laser simulation of dose-rate effects[J]. IEEE Transactions on Nuclear Science, 2018, 65(12): 2 852-2 861.

[7] CAO W, WANG L, LI T, et al. Laser simulation of transient ionizing radiation effects in the 0.18 μm CMOS inverter chain[C]// 2019 3rd International Conference on Radiation Effects of Electronic Devices (ICREED). Chongqing: IEEE, 2019.

[8] CAO W, ZHAO Y, WANG L, et al. Laser simulation of transient ionizing radiation effects in the double-power integrated circuit[C]// 2020 IEEE 3rd International Conference on Electronics Technology (ICET). Chengdu: IEEE, 2020.

[9] YUAN L, DENG H, LI S, et al. Unified theory of direct or indirect band-gap nature of conventional semiconductors[J]. Physical Review B, 2018, 98(24): 245203.

[10] CLAEYS C, SIMOEN E. Radiation effects in advanced semiconductor materials and devices [M]. Germany: Springer Science & Business Media, 2002.

[11] YAKIMOV E B, POLYAKOV A Y, SHCHEMEROV I V, et al. Experimental estimation of electron-hole pair creation energy in β-Ga_2O_3[J]. Applied Physics Letters, 2021, 118(20): 202106.

[12] NIKIFOROV A Y, SKOROBOGATOV P K. Physical principles of laser simulation for the transient radiation response of semiconductor structures, active circuit elements, and circuits: A linear model[J]. Russian Microelectronics, 2004, 33(2): 68-79.

[13] ALEXANDER D R. Transient ionizing radiation effects in devices and circuits[J]. IEEE Transactions on Nuclear Science, 2003, 50(3): 565-582.

[14] LIN M E, MA Z, HUANG F, et al. Low resistance ohmic contacts on wide band-gap GaN[J]. Applied Physics Letters, 1994, 64(8): 1 003-1 005.

[15] FILATOVA E O, KONASHUK A S. Interpretation of the changing the band gap of Al_2O_3 depending on its crystalline form: Connection with different local symmetries[J]. The Journal of Physical Chemistry C, 2015, 119(35): 20 755-20 761.

[16] XIA X, LI J, SHARMA R, et al. Radiation damage in the ultra-wide bandgap semiconductor Ga_2O_3[J]. ECS Journal of Solid State Science and Technology, 2022, 11(9): 95001.

[17] BACH S B, MCELVANY S W. Determination of the ionization potentials of aluminum oxides via charge transfer[J]. The Journal of Physical Chemistry, 1991, 95(23): 9 091-9 094.

[18] WIETS M, WEINELT M, FAUSTER T. Electronic structure of SiC(0001) surfaces studied by

two-photon photoemission[J]. Physical Review B, 2003, 68(12): 125321.

[19] WRBANEK J D, WRBANEK S Y, FRALICK G C, et al. Micro-fabricated solid-state radiation detectors for active personal dosimetry[R]. USA: NASA, 2007.

[20] HEERA V, PROKERT F, SCHELL N, et al. Density and structural changes in SiC after amorphization and annealing[J]. Applied Physics Letters, 1997, 70(26): 3 531-3 533.

[21] SHIBATA H, WASEDA Y, OHTA H, et al. High thermal conductivity of gallium nitride (GaN) crystals grown by HVPE process[J]. Materials Transactions, 2007, 48(10): 2 782-2 786.

[22] OSIPOV A V, SHAROFIDINOV S S, OSIPOVA E V, et al. Growth and optical properties of Ga_2O_3 layers of different crystalline modifications [J]. Coatings, 2022, 12(12): 1 802.

[23] AHMAD I, UNWIN M, CAO H, et al. Multi-walled carbon nanotubes reinforced Al_2O_3 nanocomposites: Mechanical properties and interfacial investigations[J]. Composites Science and Technology, 2010, 70(8): 1 199-1 206.

[24] MELINGER J S, BUCHNER S, MCMORROW D, et al. Critical evaluation of the pulsed laser method for single event effects testing and fundamental studies[J]. IEEE Transactions on Nuclear Science, 1994, 41(6): 2 574-2 584.

[25] NIKIFOROV A, SKOROBOGATOV P K. Physical principles of laser simulation for the transient radiation response of semiconductor structures, active circuit elements, and circuits: A nonlinear model[J]. Russian Microelectronics, 2006, 35: 138-149.

[26] BORSHCH A A, STARKOV V N, VOLKOV V I, et al. Optical limiting effects in nanostructured silicon carbide thin films[J]. Quantum Electronics, 2013, 43(12): 1 122.

[27] KELLY M K, AMBACHER O, DAHLHEIMER B, et al. Optical patterning of GaN films[J]. Applied Physics Letters, 1996, 69(12): 1 749-1 751.

[28] APEL O, MANN K, ZOELLER A, et al. Nonlinear absorption of thin Al_2O_3 films at 193 nm [J]. Applied Optics, 2000, 39(18): 3 165-3 169.

[29] SUN C, HUANG Y, LIANG J, et al. Large near resonance third order nonlinearity in GaN [J]. Optical and Quantum Electronics, 2000, 32: 619-640.

[30] MUTH J F, LEE J H, SHMAGIN I K, et al. Absorption coefficient, energy gap, exciton binding energy, and recombination lifetime of GaN obtained from transmission measurements[J]. Applied Physics Letters, 1997, 71(18): 2 572-2 574.

[31] SRIDHARA S G, DEVATY R P, CHOYKE W J. Absorption coefficient of 4H silicon carbide from 3 900 to 3 250 Å[J]. Journal of Applied Physics, 1998, 84(5): 2 963-2 964.